WATER RESOURCES RESEARCH, VOL. 23, NO. 12, PAGES 2175–2186, DECEMBER 1987

Soil Heat and Water Flow With a Partial Surface Mulch

SANG-OK CHUNG[1] AND ROBERT HORTON

Department of Agronomy, Iowa State University, Ames

A computer model using the alternating direction implicit (ADI) finite difference method to study two-dimensional coupled soil heat and water flow with a partial surface mulch cover is developed. A new, simplified computational procedure, which has only tridiagonal matrix problems, for the ADI method is introduced. The model uses a soil surface energy balance equation to determine soil surface boundary conditions for both heat and water flow. The inputs required for the computer simulations are weather data, soil thermal and hydraulic properties, and mulch data. Numerical experiments are performed to examine the effects of soil type, mulch width, and weather conditions on soil heat and water movement. For continuous evaporation and drainage, 10-day simulations were performed for each combination of clay, loam, and sand soil and fractions of mulch cover of 0, 0.5, 0.8, and 1.0 of the row interval width. For repetitive evaporation and infiltration, 15-day simulations were performed. The mulch cover greatly reduces evaporation loss and the amplitude of daily soil temperature, water content, and pressure head variations. Large spatial variations in temperature and soil water content are predicted near the interface of mulch and bare soil surface. The soil hydraulic properties have important roles in controlling soil surface water content. The present model reasonably describes the soil thermal and hydrologic environments and thus can be applied successfully in soil science and groundwater hydrology and can be extended to related disciplines.

INTRODUCTION

A mulch influences the soil surface radiation balance, the soil water evaporation rate, the soil temperature distribution, and the moisture distribution in the soil. The mulch can be effectively used to reduce soil erosion in humid areas and to reduce water loss by evaporation in arid areas. Several studies have been made on the effects of various soil surface mulchings on the temperature and (or) water distribution in the soil. *Mahrer* [1979] studied one-dimensional soil heat flow with a transparent polyethylene mulch present. *Mahrer and Katan* [1981] did research on two-dimensional soil heat flow when a transparent polyethylene mulch constrained the evaporation heat loss from a portion of the soil surface. *Mahrer et al.* [1984] studied one-dimensional heat and water flow when a transparent polyethylene mulch covered the entire surface. *Jury and Bellantuoni* [1976*a*, *b*] studied the soil heat and water environment affected by rocks on the soil surface. *Horton et al.* [1984*a*, *b*] studied two-dimensional soil heat transfer with incomplete soil surface plant cover. They used an explicit finite difference method to solve the heat conduction equation. The agreement between the predicted and observed temperatures in the soil profile was good.

Most previous studies were for one-dimensional vertical flow regions. In agricultural practice, a partial soil surface mulch may be applied, and two-dimensional models should be used for more realistic simulation studies of heat and water transfer. In addition, because heat and water in the soil interact with each other, a coupled heat and water flow model should be used. *Philip and De Vries* [1957] presented theory to describe coupled heat and water flow in soil. *Van Bavel and Hillel* [1975, 1976], *Sophocleous* [1979], and *Milly* [1982] expanded and (or) used the theory to calculate heat and water flow in soil.

An alternating direction implicit (ADI) finite difference model of soil heat and water flow is developed to study the effects of a partial crop residue mulch on the soil temperature and water distributions in more detail than in previous investigations. The method is physically based and general in that soil thermal and hydraulic properties and standard meteorological data are the required inputs. This model extends the model of *Horton et al.* [1984*b*] by including water flow and by replacing the canopy shading portion with a partial surface mulch condition.

Simulation runs are made by using variable soil, mulch, and weather conditions. Ten-day simulations of soil heat and water flow are made for simultaneous evaporation and drainage conditions, and 15-day simulations are made for alternating evaporation, infiltration, and drainage. The results of the selected simulation runs are reported in graphical and tabular forms for both the thermal and the hydraulic environments.

MATHEMATICAL MODEL

Flow Region

The numerical model describes a system consisting of soil layer, mulch layer, and atmospheric layer. The crop residue mulch strips are assumed to be parallel and equally spaced. A schematic description of the flow region is given in Figure 1, which shows the cross section perpendicular to the row direction. Because of symmetry, one section of the region, section *ABCD*, was considered in the model study. A rectangular coordinate system is used with origin *A* at the upper left corner of the flow region, *x* horizontally to the right, and *z* vertically downward.

Flow Equations

The flow equations governing the unsteady simultaneous heat and water flow were developed by *Philip and De Vries* [1957] as follows:

$$C\frac{\partial T}{\partial t} = \nabla\cdot(\lambda\nabla T) - L\nabla\cdot(D_{\theta v}\nabla\theta) \qquad (1)$$

$$\frac{\partial \theta}{\partial t} = \nabla\cdot(K\nabla h) - \frac{\partial K}{\partial z} \qquad (2)$$

[1]Now at Department of Agricultural Engineering, Kyungpook National University, Korea.

Paper number 6W4470.
0043-1397/87/007W-4470$05.00

where C is volumetric soil heat capacity (J/m^3 °C), T is soil temperature (°C), t is time (s), λ is thermal conductivity (W/m °C), L is volumetric latent heat of vaporization (J/m^3), θ is volumetric water content (m^3/m^3), $D_{\theta v}$ is isothermal vapor diffusivity (m^2/s), K is hydraulic conductivity (m/s), h is pressure head (m), z is the vertical distance, positive downward (m), and ∇ is gradient operator.

In the present study, the effects of water vapor on heat and moisture transport are included only at the soil surface. Subsurface vapor flow is not included, thus the model is best applied to humid and subhumid regions where prolonged drought periods that manifest subsurface vapor transport are less frequent. Consequently, (1) was changed to:

$$C \frac{\partial T}{\partial t} = \nabla \cdot (\lambda \nabla T) \tag{3}$$

Equation (2) can be modified as follows:

$$\left(\frac{\partial \theta}{\partial h}\right)_T \frac{\partial h}{\partial t} + \left(\frac{\partial \theta}{\partial T}\right)_h \frac{\partial T}{\partial t} = \nabla \cdot (K \nabla h) - \frac{\partial K}{\partial z} \tag{4}$$

where h is pressure head (m) and K is hydraulic conductivity (m/s). In this study the thermal liquid flow is assumed to be insignificant, as demonstrated by *Milly* [1984] for most soil water contents except very wet conditions, and (4) is reduced to

$$F \frac{\partial h}{\partial t} = \nabla \cdot (K \nabla h) - \frac{\partial K}{\partial z} \tag{5}$$

ADI Finite Difference Equations

Finite difference equations can be derived by replacing the differentials in (3) and (5) by difference expressions. For two-dimensional flow problems, the ADI method has been used successfully [*Selim and Kirkham*, 1973]. In the ADI method the finite difference equation is set up using one dimension implicit while leaving the other dimension explicit at a time and then changing the direction in the next time step.

The governing equations (3) and (5) can be changed into the ADI finite difference equations as follows:

$$C_{i,j}^{n+1/2} \frac{T_{i,j}^{n+1} - T_{i,j}^{n}}{\Delta t} = \frac{\lambda_{i,j+1/2}^{n+1/2}(T_{i,j+1}^{n+1} - T_{i,j}^{n+1}) - \lambda_{i,j-1/2}^{n+1/2}(T_{i,j}^{n+1} - T_{i,j-1}^{n+1})}{(\Delta x)^2} + \frac{\lambda_{i+1/2,j}^{n+1/2}(T_{i+1,j}^{n} - T_{i,j}^{n}) - \lambda_{i-1/2j}^{n+1/2}(T_{i,j}^{n} - T_{i-1,j}^{n})}{(\Delta z)^2} \tag{6}$$

$$F_{i,j}^{n+1/2} \frac{h_{i,j}^{n+1} - h_{i,j}^{n}}{\Delta t} = \frac{K_{i,j+1/2}^{n+1/2}(h_{i,j+1}^{n+1} - h_{i,j}^{n+1}) - K_{i,j-1/2}^{n+1/2}(h_{i,j}^{n+1} - h_{i,j-1}^{n+1})}{(\Delta x)^2} + \frac{K_{i+1/2,j}^{n+1/2}(h_{i+1,j}^{n} - h_{i,j}^{n}) - K_{i-1/2,j}^{n+1/2}(h_{i,j}^{n} - h_{i-1,j}^{n})}{(\Delta z)^2} - \frac{K_{i+1,j}^{n+1/2} - K_{i-1,j}^{n+1/2}}{2\Delta z} \tag{7}$$

for the odd traverse (x direction), and

$$C_{i,j}^{n+3/2} \frac{T_{i,j}^{n+2} - T_{i,j}^{n+1}}{\Delta t} = \frac{\lambda_{i,j+1/2}^{n+3/2}(T_{i,j+1}^{n+1} - T_{i,j}^{n+1}) - \lambda_{i,j-1/2}^{n+3/2}(T_{i,j}^{n+1} - T_{i,j-1}^{n+1})}{(\Delta x)^2} + \frac{\lambda_{i+1/2,j}^{n+3/2}(T_{i+1,j}^{n+2} - T_{i,j}^{n+2}) - \lambda_{i-1/2,j}^{n+3/2}(T_{i,j}^{n+2} - T_{i-1,j}^{n+2})}{(\Delta z)^2} \tag{8}$$

$$F_{i,j}^{n+3/2} \frac{h_{i,j}^{n+2} - h_{i,j}^{n+1}}{\Delta t} = \frac{K_{i,j+1/2}^{n+3/2}(h_{i,j+1}^{n+1} - h_{i,j}^{n+1}) - K_{i,j-1/2}^{n+3/2}(h_{i,j}^{n+1} - h_{i,j-1}^{n+1})}{(\Delta x)^2} + \frac{K_{j+1/2,j}^{n+3/2}(h_{i+1,j}^{n+2} - h_{i,j}^{n+2}) - K_{i-1/2,j}^{n+3/2}(h_{i,j}^{n+2} - h_{i-1,j}^{n+2})}{(\Delta z)^2} - \frac{K_{i+1,j}^{n+3/2} - K_{i-1,j}^{n+3/2}}{2\Delta z} \tag{9}$$

for the even traverse (z direction). The superscripts represent time and steps, subscripts space steps, i the row index, and j the column index, and F is the specific water capacity. Figure 2 shows the finite difference discretization of the flow region.

At each traverse, (6) and (7), and (8) and (9) have $2(M)(N)$ simultaneous equations with $2(M)(N)$ unknowns, T and h at each node, where M and N are the numbers of columns and rows in the flow region, respectively. In principle, the equations (6) and (7) for the odd traverse and (8) and (9) for the even traverse have to be solved simultaneously for each time step. That means we have to solve a $2(M)(N)$ by $2(M)(N)$ matrix, which requires a lot of computation even though the matrix is banded with a band width of six in this particular case. To reduce the computation requirements, a modified procedure was followed by solving each set of $(M)(N)$ simultaneous equations for each of (6) through (9) separately. This modification will not introduce large errors if a small time step size is used and will greatly reduce necessary computation inasmuch as, in each stage, (6) through (9) end up with a tridiagonal matrix that can be efficiently solved by using the so-called Thomas algorithm [*Lapidus and Pinder*, 1982].

Equations (6) through (9) are nonlinear because the values of coefficients are dependent on the values of the variables themselves. Therefore an iteration method can be used when solving these equations. However, if the time step size is small, the coefficients in (6) through (9) can be approximated by using values from the previous time step such as

$$\lambda^{n+1/2} = \lambda^{n} \tag{10}$$

$$\lambda^{n+3/2} = \lambda^{n+1} \tag{11}$$

This simplifies the computations because the system of equations becomes linear.

The computational procedure for determining temperature and pressure head is as follows: (1) determine the values of coefficients by using values of variables at time step n, (2) compute T^{n+1} using T^{n} (equation 6), (3) compute h^{n+1} using h^{n} (equation 7), (4) determine the values of coefficients by using values of variables at time step $n + 1$, (5) compute T^{n+2} using

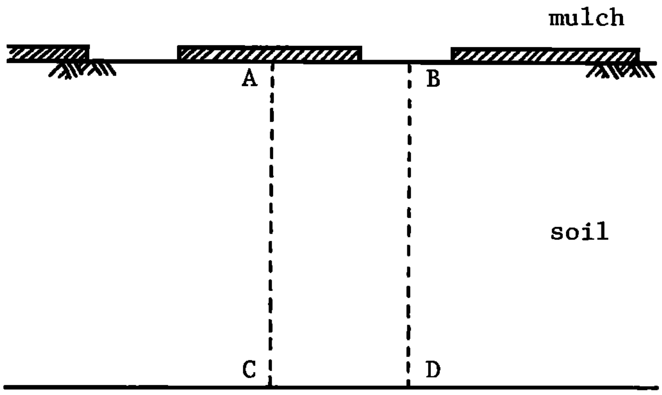

Fig. 1. Schematic diagram of the flow region.

T^{n+1} (equation 8), and (6) compute h^{n+2} using h^{n+1} (equation 9).

The internodal coefficients such as hydraulic conductivity and thermal diffusivity as shown in (6) through (9) were determined by using the geometric mean of the two neighboring nodes because it was shown that the geometric mean gave more realistic results than did the arithmetic mean [*Haverkamp and Vauclin*, 1979; *Schnabel and Richie*, 1984].

Initial and Boundary Conditions

Specific conditions, namely the initial and boundary conditions, are needed to solve the flow equations. The initial condition includes variable values for each node in the flow region at the beginning of the simulation. Boundary conditions can be either one of a flux condition or a value-specified condition, or the combination of the two. These boundary conditions are mathematically termed Neumann condition, Dirichlet condition, and Cauchy condition, respectively. To effectively handle the flux boundary condition is the most difficult part in the finite difference method. Therefore most of the previous studies used value-specified boundary conditions, which are simpler to handle than flux boundary conditions.

A no-flow boundary condition is a special case of the flux boundary condition and is much easier to handle than the nonzero flux boundary condition. In the present study, value-specified boundary conditions were used for the top and bottom boundary conditions for the heat flow, no-flow boundary conditions for right and left boundaries for both heat and water flow, and nonzero flux boundary conditions for top and bottom boundaries for water flow. The soil surface boundary conditions for both heat and water flow are not explicitly known (input), but are implicitly determined by energy partitioning (discussed in Energy Balance Equation section).

There is a special requirement to keep a high accuracy in the ADI method for the intermediate time step boundary conditions for time dependent boundary conditions as described by *Lapidus and Pinder* [1982, pp. 251–253]. However, that requirement can be satisfied only for explicit value-specified boundary conditions. In this study, since the boundary condition, either value or flux condition, is implicitly determined by energy balance equation, the special requirement cannot be satisfied. At the intermediate time step, the boundary condition at the previous time step was assumed.

When employing value-specified boundary conditions, the value at each specified time is placed directly into the finite difference equation. To handle the flux boundary conditions in the finite difference method, imaginary nodes are introduced outside the flow regime [*Lapidus and Pinder*, 1982; *Gilding*, 1983]. For example, the flux at node 1 can be expressed in finite difference form as

$$\text{flux} = -A(H_2 - H_0)/2\Delta z \tag{12}$$

where A is thermal or hydraulic conductivity and H is total head or temperature. Subscript 0 represents an imaginary node outside node 1. For a no-flux boundary, (12) equals zero, hence $H_2 = H_0$. Therefore an expression for the imaginary point, H_0, can be simply replaced by H_2 in (6) to (9). For a nonzero flux boundary, solve (12) for the imaginary point, H_0, then replace H_0, which is expressed in terms of H_2 and the flux, in (6) to (9). The flux at node N can be handled similarly.

The soil surface temperature and evaporation rate were determined by using an energy balance equation for the soil surface during dry weather. Infiltration rate and soil surface temperature during the rainy weather were determined from Darcy's equation and air temperature, respectively. In the energy balance approach, there is no need to worry about the potential and actual evaporation rates because the method directly calculates actual evaporation. However, the potential infiltration rate is governed by rainfall amount, whereas the actual rate is governed by both rainfall amount and soil infiltrability. Those two should be compared, and the smaller governs the actual infiltration rate. A unit gradient of total head was used for the water flow bottom boundary condition.

Energy Balance Equation

Soil surface temperature and evaporation rate were determined implicitly from the partitioning of the surface energy. A procedure described by *Van Bavel and Hillel* [1975, 1976] and

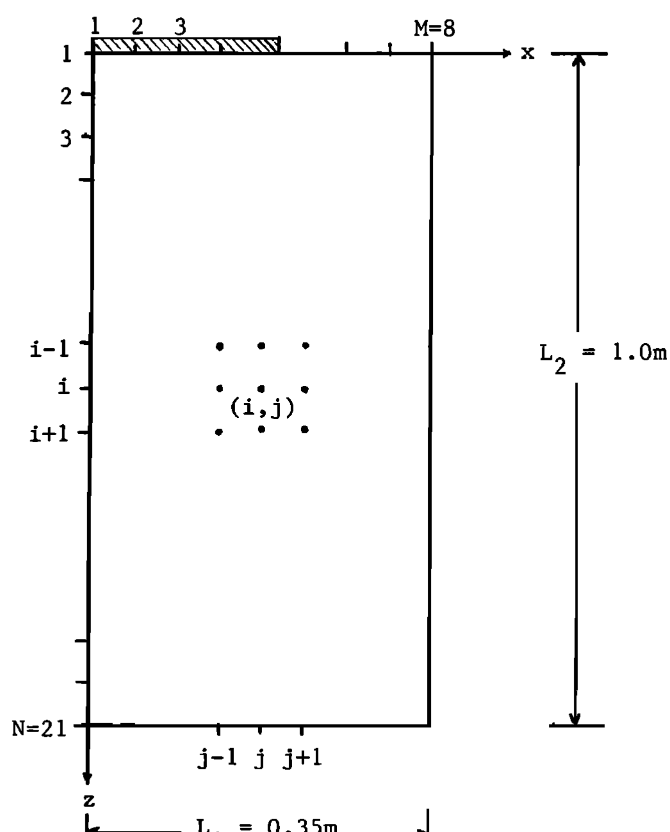

Fig. 2. Finite difference discretization of the flow region.

Horton [1984b] was used. The energy balance at the soil surface for bare soil is described by

$$R_n - H_s - LE - G = 0 \tag{13}$$

where R_n is net radiation (positive downward), H_s is sensible air heat flux (positive upward), LE is latent heat flux (positive upward), and G is soil heat flux (positive downward).

The value of R_n is found as

$$R_n = (1 - al)R_g + R_1 - \varepsilon\sigma(T_s + 273.16)^4 \tag{14}$$

where R_g(W/m^2) is the measured global radiation, R_1(W/m^2) is the long-wave sky irradiance, T_s is the surface temperature (°C), al is the soil surface albedo, ε is the emissivity, and σ(W/m^2 °K^4) is the Stefan-Boltzmann constant. R_1 is calculated as was done by *Van Bavel and Hillel* [1976] from the following form of Brunt's formula:

$$R_1 = \sigma(T_a + 273.16)^4[0.605 + 0.048(1370\ H_a)^{12}] \tag{15}$$

where T_a is air temperature (°C) and H_a is the air humidity (kg/m^3).

The latent and sensible heat fluxes at the surface were calculated by using the following equations:

$$E = (H_0 - H_a)/(1000\ r_a) \tag{16}$$

$$L = 2.4946(10^9) - 2.247(10^6)T_s \tag{17}$$

$$LE = L\ E \tag{18}$$

$$H_s = \rho_a c_{pa}(T_s - T_a)/r_a \tag{19}$$

where E is the evaporative flux (m/s), L is volumetric latent heat of vaporization (J/m^3) given by *Forsythe* [1964], H_0 is the absolute humidity of air at the soil surface (kg/m^3), H_a is the absolute humidity of air above soil surface (kg/m^3), r_a is the aerodynamic boundary layer resistance between the soil surface and the air above it (s/m), ρ_a is air density (kg/m^3), c_{pa} is specific heat of air at constant pressure (J/kg °C).

The absolute humidity, H_0, and aerodynamic resistance were calculated by using the following equations [*Van Bavel and Hillel*, 1976]:

$$H_0 = H_0^* \exp\ [h_1/46.97(T_s + 273.16)] \tag{20}$$

$$r_a = [\ln\ (2.0/Z_0)]^2/0.16W_s \tag{21}$$

where H_0^* is the saturation humidity at the soil surface temperature (kg/m^3), h_1 is the pressure head at the surface (m), Z_0 is roughness length (m), and W_s is the wind speed (m/s). In (20), H_0 depends not only upon the surface temperature but also on the surface water content, and h_1 cannot be greater than zero in (20).

The absolute humidity of air, H_a, and the saturation humidity at the soil surface temperature, H_0^*, were calculated by the following equations:

$$H_a = 1.323\ \exp\ [17.27\ T_d/(T_d + 237.3)]/(T_a + 273.16) \tag{22}$$

$$H_0^* = 1.323\ \exp\ [17.27\ T_s/(T_s + 237.3)]/(T_s + 273.16) \tag{23}$$

where T_d is the dewpoint temperature (°C).

The soil heat flux at the soil surface was determined by

$$G = \lambda \frac{T_s - T_2}{\Delta z} + \rho_s c_{ps}(T_s - T_s^\circ)\frac{\Delta z}{2\Delta t} \tag{24}$$

where λ is thermal conductivity (W/m °C), T_s is unknown temperature on the soil surface (°C), T_s° is T_s at previous time step (°C), T_2 is temperature at node Δz below the soil surface at previous time step (°C), ρ_s is soil density (kg/m^3), c_{ps} is specific heat of soil at constant pressure (J kg/°C), Δz is step size in z direction (m), and Δt is time step (s). Equation (24) approximates the soil heat flux density by summing a term that estimates soil heat flux at a depth of $\Delta z/2$ and a term that estimates the change in heat stored in the soil above $\Delta z/2$. The second term on the right-hand side is a corrective term to compensate the error in the first term for the relatively large step size of Δz.

For a mulched surface, additional consideration should be given. The energy balance equation should be applied at both the mulch surface and at the mulch-soil interface as described by *Van Bavel and Hillel* [1975]. In this analysis we assume nontransparent mulch cover such that radiation does not penetrate below the surface. For the top of the mulch surface, the energy balance equation is

$$R_n - H_s - M_s = 0 \tag{25}$$

where R_n and H_s are the same as (13) and M_s is the mulch heat flux (positive downward). The H_s can be determined as

$$H_s = \rho_a c_{pa}(T_m - T_a)/r_a \tag{26}$$

$$M_s = \lambda_m(T_m - T_s)/THK \tag{27}$$

where T_m is temperature on the mulch surface (°C), λ_m is thermal conductivity of mulch layer (W/m°C), THK is the thickness of mulch layer (m), and the others are the same as previously defined.

For the mulch-soil interface, the energy balance equation is

$$M_s - LE - G = 0 \tag{28}$$

The latent heat flux on the soil surface was calculated by using (17) and (18) with

$$E = (H_0 - H_a)/[1000(r_a + r_m)] \tag{29}$$

where all are the same as in (16) with an additional term r_m, the diffusion resistance (s/m) of the mulch. The r_m is determined by [*Hillel et al.*, 1975]:

$$r_m = THK/D_{\text{atm}}f\tau \tag{30}$$

where THK is the thickness of the mulch layer, D_{atm} is the vapor diffusivity in air (m^2/s), f is the mulch porosity, and τ is tortuosity factor. This analysis does not consider convective transport of gas within the mulch layer, which, if present, will act to decrease r_m.

To determine the soil surface temperature and evaporation rate, the energy balance equation was solved. For bare soil, (14), (18), (19), and (24) were substituted into (13). All these equations are unknown functions of T_s. Therefore an iterative root-finding method is used to solve Eq. (13) for T_s (the surface temperature). The bisect method was used for root finding. The T_s value from the previous time step was used as an initial guess, and the iteration was continued until the difference of T_s in successive iteration was less than a predetermined tolerance. When T_s was determined, the evaporation rate was also determined by (16).

For mulched soil, (14), (26), and (27) are substituted into (25). Then, the same procedure as in the bare soil was followed to determine the mulch surface temperature, T_m, and mulch heat flux, M_s. With this M_s as an input, (17), (24), (27), and (29) are substituted into (28) to determine the mulch-soil interface temperature, T_s. The same iterative procedure as in the bare soil was followed to determine T_s. As soon as T_s is determined, the evaporation rate is also determined by (29).

Inputs Required for Computer Simulation

Specific weather, mulch, and soil parameters are required as inputs to solve soil heat and water flow problems. The weather inputs are daily global radiation, maximum and minimum air temperature, maximum and minimum dewpoint temperature, and average daily windspeed. The weather inputs are those at the height of 2 m above the ground. The mulch inputs are width, thickness, thermal conductivity, moisture diffusion resistance, porosity, and tortuosity factor. Soil parameters required as inputs are initial temperature and water content distributions, lower boundary temperature and water content as a function of time, soil surface emissivity as a function of water content, soil surface albedo as a function of water content, soil thermal diffusivity as a function of water content, soil water hydraulic conductivity as a function of water content, specific water capacity as a function of water content, and the soil-water characteristic curve.

A few general inputs are also required to run the computer program. The inputs are as follows: L_1, L_2, Δz, Δx, solar noon, daylength, time length of simulation, Δt (incremental time step), and Z_0 (the surface roughness length).

The weather inputs are used in conjunction with empirical expressions to describe the weather conditions as a function of time. Global radiation as a function of time for soil in direct sunlight is described as

$$R_g = (\pi/2)\ DR/DL \sin\left[(t - SN + DL/2)\ \pi/DL\right] \quad (31)$$

where R_g is in W/m^2, DR is daily global radiation (J/m^2), t is time of a day (s), SN is solar noon (s), and DL is daylength (s). Equation (31) distributes the daily radiation during the daytime by using a sine function. The air temperature and dewpoint temperature were also determined by sine functions as follows:

$$T_a = \bar{T}_a + A_a \sin(2\pi t/86400 + \pi) \quad (32)$$

$$T_d = \bar{T}_d + A_d \sin(2\pi t/86400 + \pi) \quad (33)$$

where the bar represents the average and A represents amplitude, and t is time of a day beginning from midnight (s). The π was included to allow the highest air temperature to be at noon.

Soil surface emissivity, ε, follows that used by *Van Bavel and Hillel* [1976],

$$\varepsilon = 0.9 + 0.18\ \theta \quad (34)$$

Soil surface albedo, al, follows that used by *Van Bavel and Hillel* [1976],

$$\begin{aligned} al &= 0.35 - \theta \qquad 0.10 \leq \theta \leq 0.25 \\ al &= 0.10 \qquad 0.25 \leq \theta \\ al &= 0.25 \qquad \theta \leq 0.10 \end{aligned} \quad (35)$$

Thermal conductivity is described by a simple empirical equation:

$$\lambda(\theta) = b_1 + b_2\theta + b_3\theta^{0.5} \quad (36)$$

where λ is thermal conductivity (W/m °C), θ is volumetric water content (m^3/m^3), and b_1, b_2, and b_3 are the regression parameters.

The volumetric soil heat capacity is determined by following *De Vries* [1963] as

$$C = 1.92 \times 10^6\ x_s + 2.51 \times 10^6\ x_o + 4.18 \times 10^6\ \theta \quad (37)$$

Where C is in J/m^3 °C, x_s and x_o are volume fractions of solid and organic matter in the soil, and θ is the volumetric water content. Soil water characteristics, hydraulic conductivity, and specific water capacity are described by empirical equations presented by *Van Genuchten* [1980] as follows:

$$\theta = \theta_r + (\theta_s - \theta_r)\left[\frac{1}{1 + (ah)^n}\right]^{1-(1/n)} \quad (38)$$

$$K(h) = K_s \frac{\{1 - (ah)^{n-1}[1 + (ah)^n]^{(1-n)/n}\}^2}{[1 + (ah)^n]^{(n-1)/2n}} \quad (39)$$

$$F(\theta, h) = (n - 1)(\theta - \theta_r)\left[1 - \left(\frac{\theta - \theta_r}{\theta_s - \theta_r}\right)^{n/(n-1)}\right]\Big/ h \quad (40)$$

where θ_s and θ_r are saturated and residual water content, K_s is saturated hydraulic conductivity at the reference temperature, h is absolute value of pressure head, and a and n are nonlinear regression parameters describing the shape of the soil water characteristic curve. The hydraulic conductivity should be corrected for temperature as:

$$K(h, T) = K(h)K_t(T) \quad (41)$$

where $K_t(T) = \mu(T_0)/\mu(T)$, the temperature correction factor, μ is the viscosity, and T_0 is the reference temperature. Here the density effect is considered negligible compared to the viscosity effect.

TEST OF MODEL

The performance of a numerical model should be evaluated to examine its validity because any numerical scheme may introduce instability, truncation, and round-off errors. A model is valid only if the approximate solution is satisfactorily accurate or close to the exact solution if one exists. The accuracy of a model can be more specifically defined in terms of its convergence and stability.

Convergence is satisfied when the approximation approaches the exact solution as step sizes of the spatial and temporal discretization approach zero. A model is said to be stable if the amplification of the error is restricted or has a finite limit as computation marches forward in time. The validity of a model can be tested by comparing the numerical solution with either an analytical solution, if it is available, or observed data.

Since there is neither an analytical solution nor measured data for the two-dimensional simultaneous heat and water flow, the entire model developed here cannot be tested directly against an analytical solution or measured data. Therefore, in this paper, only the heat flow part of the ADI method is tested through comparison with an analytical solution. The heat conduction equation for a hot steel rod of semiinfinite length with a rectangular cross section being exposed to a cooling air stream was solved numerically using the ADI method and then compared with the analytical solution given by *Incropera and DeWitt* [1981, pp. 190–210]. Figure 3 shows the cross section area of the steel rod. Since the conduction heat flow is symmetrical in both directions, only one quarter of the cross section is considered in the analysis. Figure 3 also shows the x and z coordinate system and the boundary conditions of no-flux conditions along the symmetrical line and flux conditions along the outside boundaries. The dimension and thermal properties of steel rod used are 0.5 by 1.0 m, thermal conductivity of 20 W/m °K, density of 3000 kg/m^3, and specific heat

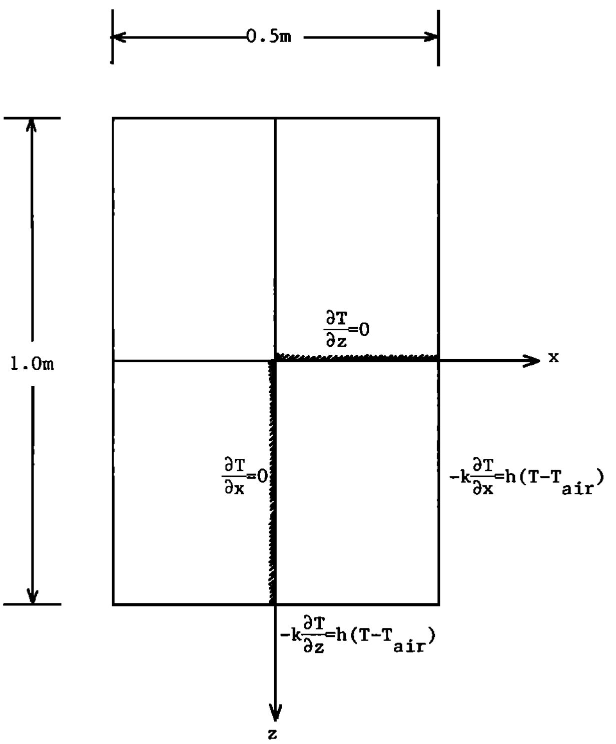

Fig. 3. Cross-section, flow region, and boundary conditions for the heat flow problem in a steel rod.

of 1000 J/kg °K. The convection heat transfer coefficient of the air stream is 10 W/m^2 °K.

The initial temperature of the steel rod is 300°C, and the air stream temperature was maintained at 20°C. A spatial step size of 0.01 m and the time step size of 5 s were used. A simulation run was made for 4000 s during which the temperature of the rod decreased near the air stream temperature.

Figure 4 shows the temperature distribution in the steel rod at the selected times as determined analytically and numerically. The ADI method is shown to compare favorably with the analytical method. Even at later times as the temperature in the steel rod approaches the air stream temperature, the agreement between the two solutions is good.

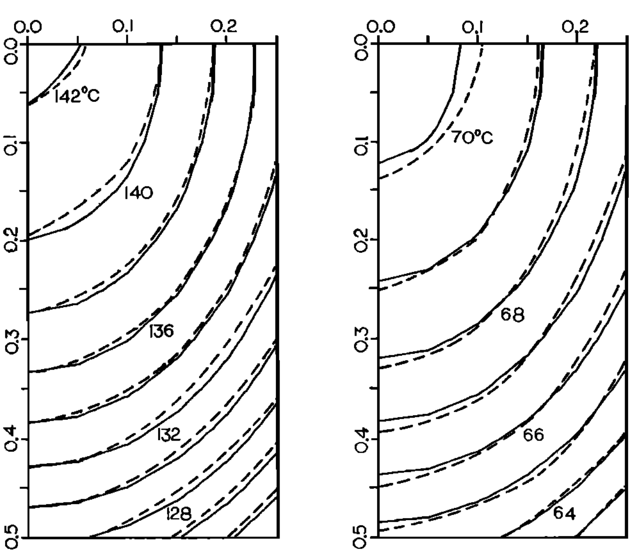

(a) at t=520 s (b) at t=1040 s

Fig. 4. Comparison of solutions of the heat flow in a steel rod between ADI solution (solid line) and analytical solution (dashed line).

TABLE 1. Hydraulic and Thermal Properties of the Soils

Parameter*	Clay	Loam	Sand
K_s (m/s)	0.2×10^{-5}	0.7×10^{-5}	2.5×10^{-5}
θ_s (m^3/m^3)	0.52	0.48	0.44
θ_r (m^3/m^3)	0.03	0.01	0.0
a (m^{-1}) in (38)	0.43	1.55	3.28
n in (38)	1.36	1.50	1.54
b_1 in (36)	−0.197	0.243	0.228
b_2 in (36)	−0.962	0.393	−2.406
b_3 in (36)	2.521	1.534	4.909

*K_s is saturation hydraulic conductivity, θ_s is saturation water content, θ_r is residual water content, a and n are parameters in Van Genuchten's retention equation, and b_1, b_2, and b_3 are parameters in thermal conductivity equation.

NUMERICAL EXPERIMENTS

Simulation runs were made using variable soil, mulch, and weather conditions. Three hypothetical soils, representing a sand, a loam, and a clay were selected for the simulations. Variable width of crop residue mulch cover and variable weather conditions were considered. Soils were assumed to be homogeneous and isotropic. The soil water retention and hydraulic conductivity relations of these soils were obtained from *Hillel and Van Bavel* [1976]. Retention data were picked up from the curves given in *Hillel and Van Bavel* [1976] and were used to determine regression parameters in Van Genuchten's retention equation (equation (38)) by graphically curve fitting as explained in *Van Genuchten* [1980].

Previously reported data were used to describe the thermal properties of these soils. To determine the empirical parameters in the thermal conductivity equation (equation (36)), data in Table 7.6 of *De Vries* [1963] and in the works by *Wierenga et al.* [1969] and *Horton and Wierenga* [1984] were used for clay, loam, and sand, respectively. Table 1 shows the thermal and hydraulic parameters for the three soils.

A mulch may vary in thickness, width, and material. In the present study, a 0.025-m-thick crop residue (corn) mulch with variable width was used. A row interval of 0.70 m was used in this study. Mulch widths of 0, 0.35, 0.55, and 0.70 m were used in the simulations. The diffusion resistance of the mulch was determined by (29), and the value of 1200 s/m was obtained. This is about an order of magnitude larger than the aerodynamic resistance between the soil surface and the air, r_a.

Various weather conditions can be used with the numerical model. In the present study, first, 10-day simulations of a dry weather condition (no rain), allowing simultaneous drainage and evaporation, were performed. Second, 15-day simulations of repeating dry and rainy weather, allowing simultaneous drainage and either evaporation or infiltration were performed. The rainfall occurred at the beginning of the third day and lasted 6 hours: 2 hours at a low steady intensity of 10 mm/hr, 2 hours at a high steady intensity of 20 mm/hr, and 2 hours at a low steady intensity of 10 mm/hr, for a total rainfall of 80 mm.

An initial condition of 20°C was used for soil temperature, and −1.1 m of soil surface pressure head with a soil-profile equilibrium condition was used for water. A bottom boundary condition of 20°C was maintained for heat flow, and a gravity flux condition was maintained for the water flow. Average daily weather input data (except for rainfall) for Des Moines, Iowa, in the month of June were used as shown by *Van Bavel and Hillel* [1976].

The flow region has width of 0.35 m, one half of the row

TABLE 2. Input Parameter Values Used in the Simulations

Parameter	Definition	Value
DAYL	Daylength	50400 s
DELX	Spatial step size in x coordinate	0.05 m
DELZ	Spatial step size in z coordinate	0.05 m
RAMDAM	Thermal conductivity of mulch	0.126 W/m °C
RGD	Daily global radiation	21.63×10^6 J/m^2
RLENG	Width of mulch cover	Variable
RM	Mulch moisture diffusion resistance	1200 s/m
SNOON	Solar noon	43200 s
TAVE	Average daily air temperature	21°C
TAMP	Amplitude of daily air temperature	5°C
TAW	Mulch tortuosity factor	0.67
TDAMP	Amplitude of daily dewpoint temperature	2°C
TDEW	Average of daily dewpoint temperature	16.4°C
THKM	Mulch thickness	0.025 m
TIMEST	Time step size	Variable
WS	Wind speed	1.69 m/s
XLENG	Length of x coordinate	0.35 m
ZLENG	Length of z coordinate	1.0 m
ZO	Soil surface roughness length	0.01 m

interval, and depth of 1.0 m. A spatial step size of 0.05 m was used for both directions. Time step sizes of 300 and 600 s were used for sand and the others, respectively, for the continuous dry weather. During and for some period after a rainfall the time step size was reduced to 1/10 to 1/200 that of dry weather. Table 2 shows the input parameter values used in the simulation.

The numerical simulation provides several descriptions for both the thermal and the hydraulic environments. Included for the thermal environment are soil temperature distribution, instantaneous and cumulative net radiation, sensible heat flux, latent heat flux, and soil heat flux at the soil surface. Included for the hydraulic environment are pressure head and water content distribution, instantaneous and cumulative infiltration, and evaporation, drainage, and storage of water in the flow region.

TABLE 3. Daily Totals of Net Radiation (R_n), Sensible Heat (S_h), Latent Heat (LE), and Soil Heat (G) and the Maximum and Minimum Temperature on the Bare Soil Surface (Node 8) of the Sand Soil With a Half-Width Mulch Cover

Day	R_n, MJ/m^2	S_h, MJ/m^2	LE, MJ/m^2	G, MJ/m^2	$T_{s,max}$, deg C	$T_{s,min}$, deg C
1	13.25	0.635	11.57	1.033	26.8	16.1
2	12.95	0.650	11.59	0.692	26.8	16.2
3	12.66	0.622	11.49	0.526	26.7	16.3
4	12.41	0.605	11.22	0.605	26.8	16.2
5	10.26	5.550	0.247	4.445	37.1	17.0
6	9.88	6.324	0.047	3.505	38.0	17.7
7	9.79	6.515	0.044	3.224	38.1	17.9
8	9.58	6.927	0.042	2.604	38.8	18.2
9	9.46	7.153	0.035	2.275	38.9	18.5
10	9.41	7.255	0.029	2.134	39.0	18.6

RESULTS AND DISCUSSION

A two-dimensional soil heat and water flow model was run for 24 particular sets of input parameters (three soils, two weather regimes, and four surface mulch widths). Input weather parameters (except rainfall) were allowed to recycle in the same manner for each day of the simulation period. The results of the computer-simulated thermal environment and hy-

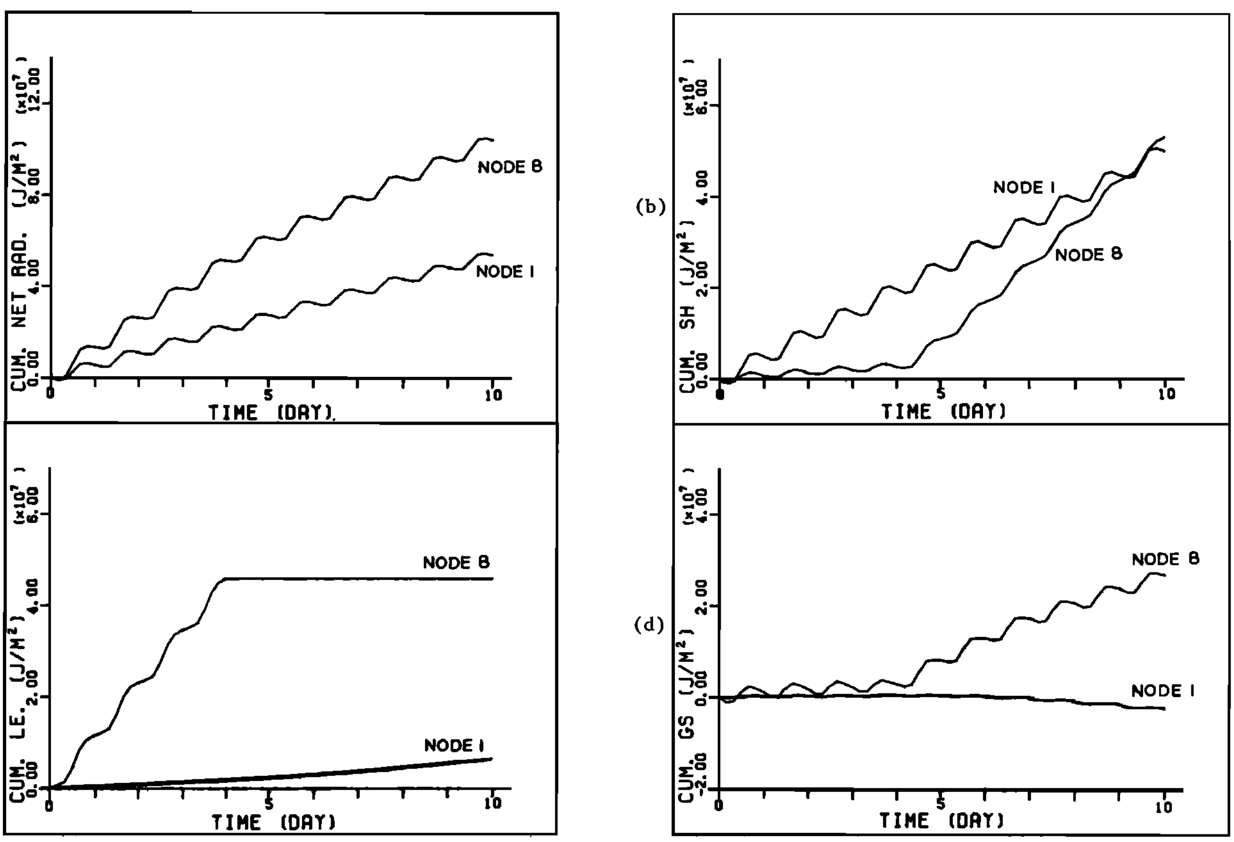

Fig. 5. Predicted cumulative heat flux of net radiation (*a*), sensible heat (*b*), latent heat (*c*), and soil heat (*d*) for the sand soil with a half-width mulch cover for a 10-day simulation.

TABLE 4. Daily Totals of Net Radiation (R_n), Sensible Heat (S_h), Latent Heat (LE), and Soil Heat (G) on Day 1 and 10 for Full Mulch and Zero Mulch (Bare) Conditions With Simultaneous Evaporation and Drainage for a 10-day Simulation

		Day 1				Day 10			
Soil	Cover	R_n, MJ/m²	S_h, MJ/m²	LE, MJ/m²	G, MJ/m²	R_n, MJ/m²	S_h, MJ/m²	LE, MJ/m²	G, MJ/m²
Clay	Mulch	5.49	4.82	0.38	0.28	5.46	4.88	0.46	0.17
	Bare	12.90	0.60	11.65	0.61	13.62	0.91	12.46	0.23
Loam	Mulch	5.49	4.82	0.38	0.30	5.46	4.87	0.46	0.14
	Bare	13.84	0.83	12.21	0.76	9.06	7.76	0.33	0.95
Sand	Mulch	5.49	4.82	0.38	0.28	5.46	4.87	0.44	0.16
	Bare	13,22	0.68	11.69	0.88	9.07	7.94	0.01	1.13

draulic environment with particular focus on two representative simulations are given in this section. The focus is on the sand soil with a half-width mulch cover without rainfall. Results from this simulation are discussed to display the ability of the model and to show the major influence of a partial mulch cover on heat and water flow. The results from the other simulations are presented in a manner to show differences and similarities relative to the simulation that received the major focus.

Thermal Environment

The results of selected simulation runs are presented in graphical form for heat flow. The 10-day simulations of simultaneous evaporation and drainage for the sand soil are discussed.

Figure 5 shows the predicted cumulative heat fluxes at the soil or mulch surfaces for the sand soil with one half of the row interval covered with mulch during a 10-day simulation. Nodes 1 and 8 represent the middle of the mulch strip and the middle of the bare soil strip, respectively. At node 1 with mulch cover, net radiation and sensible heat flux are at the mulch surface, and latent heat and soil heat flux are at the bare soil-mulch interface. The cumulative net radiation on bare soil is about twice as large as that on the mulch, partly because of the larger albedo on the mulch.

At node 1 on or under the mulch, all the cumulative heat flux curves maintain constant trend slopes for the entire period, whereas at node 8 on a bare surface, these curves change from day 5 (Figure 5). From day 5, net radiation decreases, sensible heat and soil heat flux increase, and latent heat flux becomes zero. This indicates that from day 5, little soil surface water is available for evaporation. Since the daily weather input values are the same for the simulation period, the change in heat flux from day 5 is caused by changing soil thermal properties and the partitioning of the energy formerly used for evaporating water. The rapid increase in cumulative soil heat results in very high soil surface temperatures on the bare surface.

Figure 6 shows temperature variation at the soil surface and

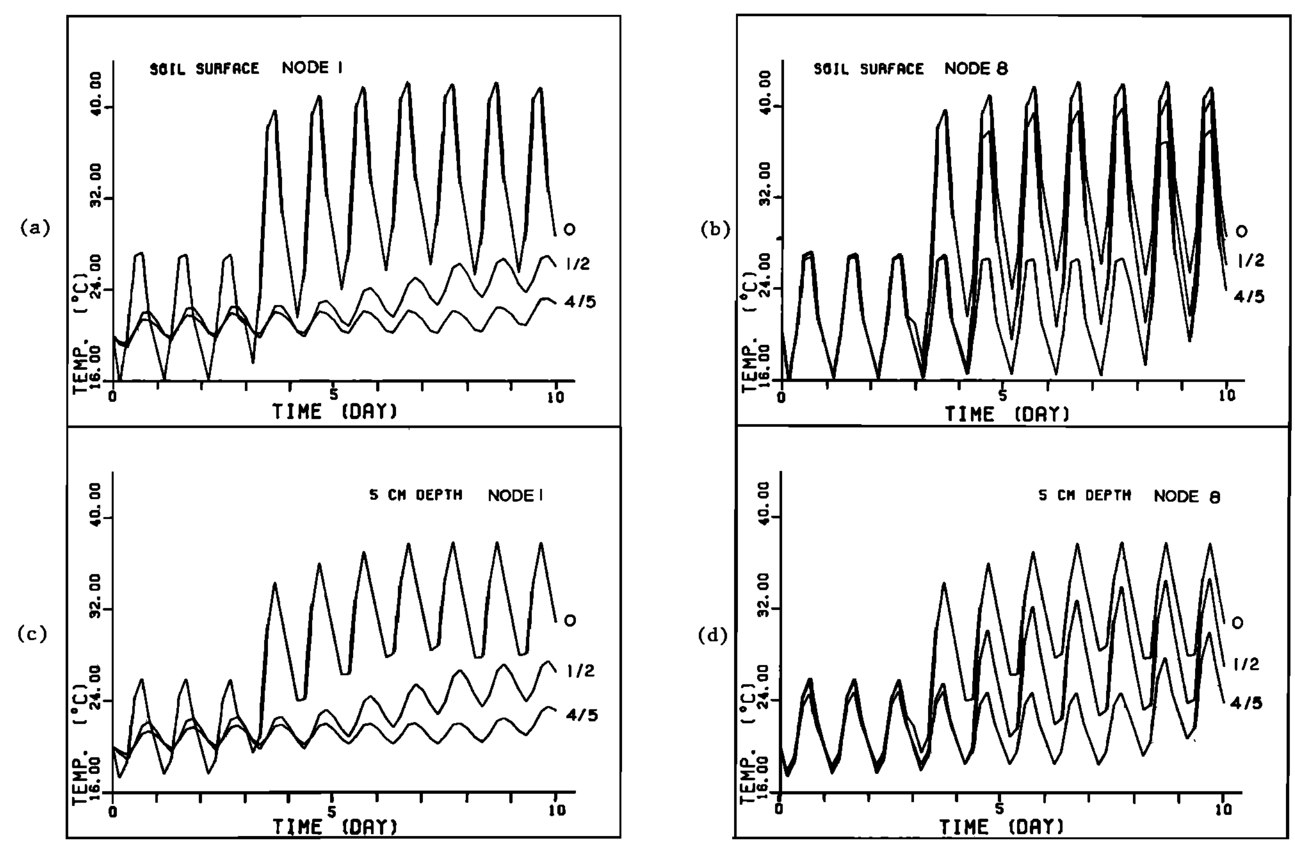

Fig. 6. Predicted soil temperature at the soil surface node 1 (*a*) and node 8 (*b*), and at the 5-cm-depth node 1 (*c*) and node 8 (*d*), for the sand soil with variable mulch cover width.

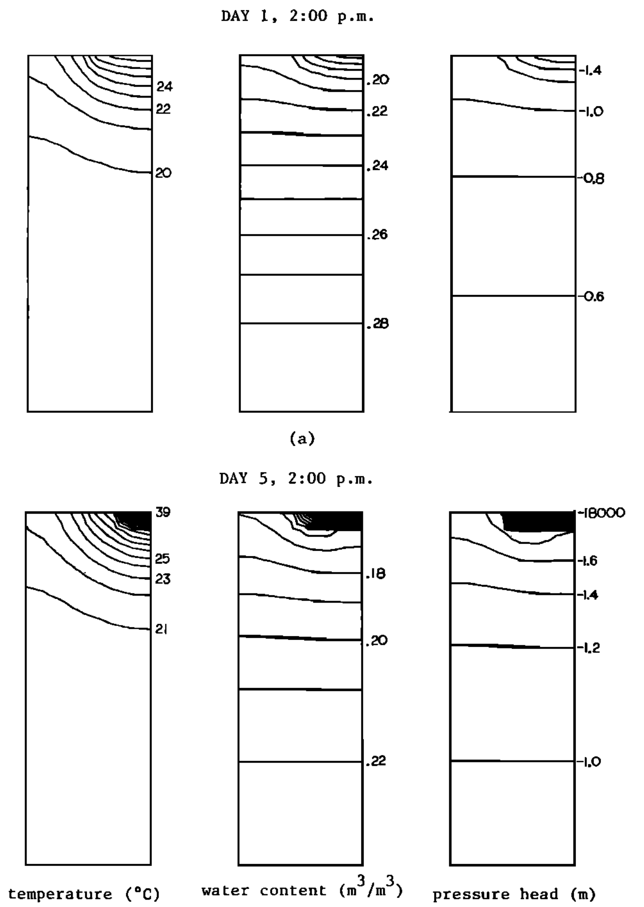

Fig. 7. Contour plots of temperature, water content, and pressure head in the 0.35 × 1.0 m flow region at 2.00 P.M. for day 1 (*a*) and day 5 (*b*) for the sand soil with a half-width mulch cover.

the 5-cm depth with variable mulch cover width. At the soil surface node 1, the trend slopes of temperature variation change from day 5 and from day 9 for a half- and a 4/5-width mulch, respectively. These correspond to a sudden increase in temperature at node 8 in Fig. 6*b*. This confirms the existence of lateral heat flow from the bare soil to the mulched soil for partly mulch covered soils. Soil temperature at the 5-cm depth responded in a manner similar to the soil surface except with smaller temperature amplitudes. Figures 6*b* and 6*d* show the effect of mulch width on the soil temperature variation. Abrupt increases in soil temperature at node 8 occur at day 4, day 5, and day 9 for zero and a half- and a 4/5 width mulch cover, respectively. These abrupt changes are coupled to the changing soil surface water contents.

Temperature and moisture content changes at the plant seed position (5-cm-depth, node 8) due to the mulch cover are important. The daily maximum and minimum temperatures at the 5-cm depth (node 8) with a half-width mulch cover show no difference from those with no mulch until day 3, and both show 5°C lower than those with no mulch from day 4 for the sand soil during a 10-day simulation. With a 4/5-width mulch cover, daily maximum and minimum temperature of the 5-cm depth (node 8) are 1°C lower and 0.5°C higher, respectively, than those with a half-width mulch cover until day 3, and are 8°C lower and 4°C lower, respectively, than those with a half-width mulch cover from day 4. For the sand soil, the temperature at the position where the plant seeds are located is very much affected by the width of mulch cover. As the mulch cover width increases, the temperature at this position decreases. This might increase the time required for germination of spring plants.

Figure 7 shows contour plots of temperature, water content, and pressure head at 2:00 P.M. for the sand soil with a half-width mulch cover. On day 1, temperature on the soil surface

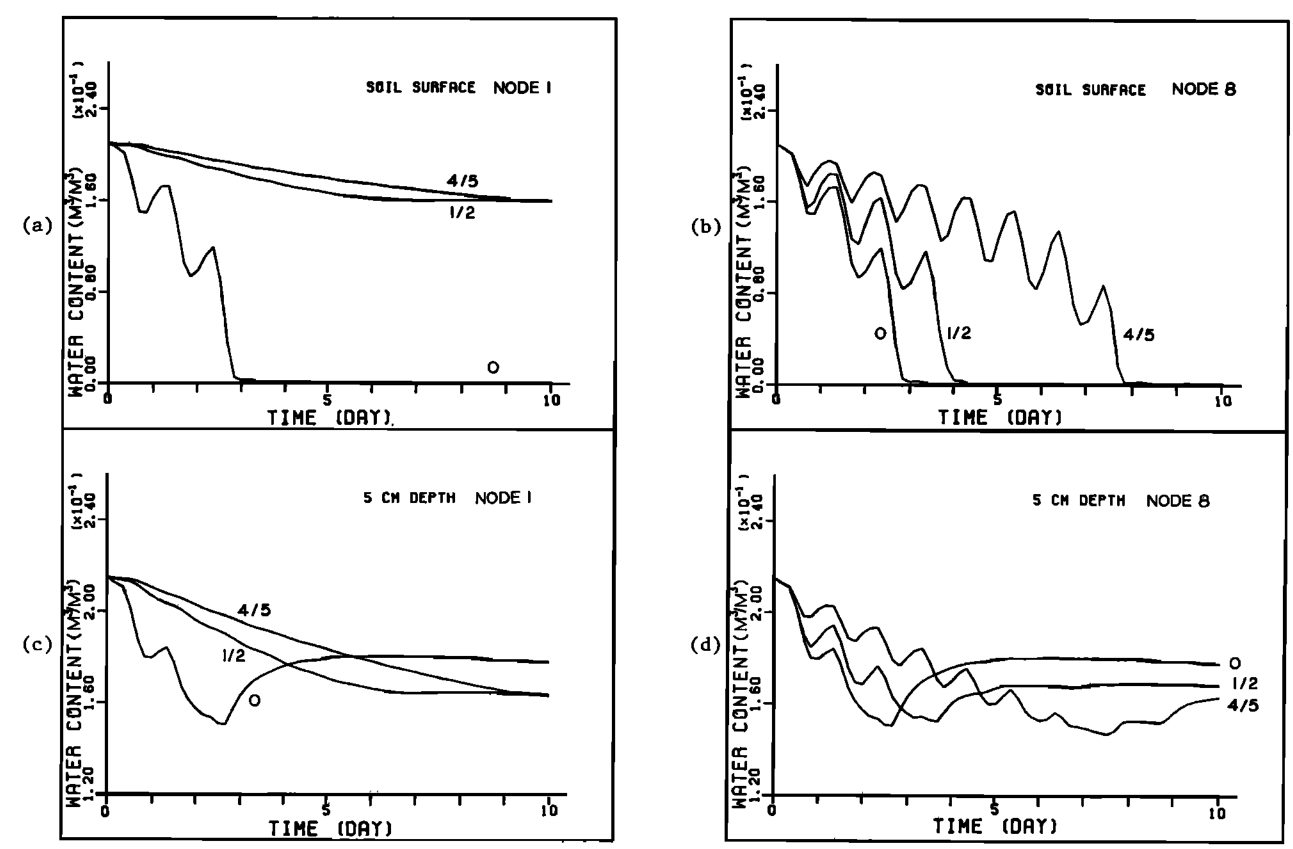

Fig. 8. Predicted water content at the soil surface node 1 (*a*) and node 8 (*b*), and at the 5-cm-depth node 1 (*c*) and node 8 (*d*), for the sand soil for variable mulch cover width.

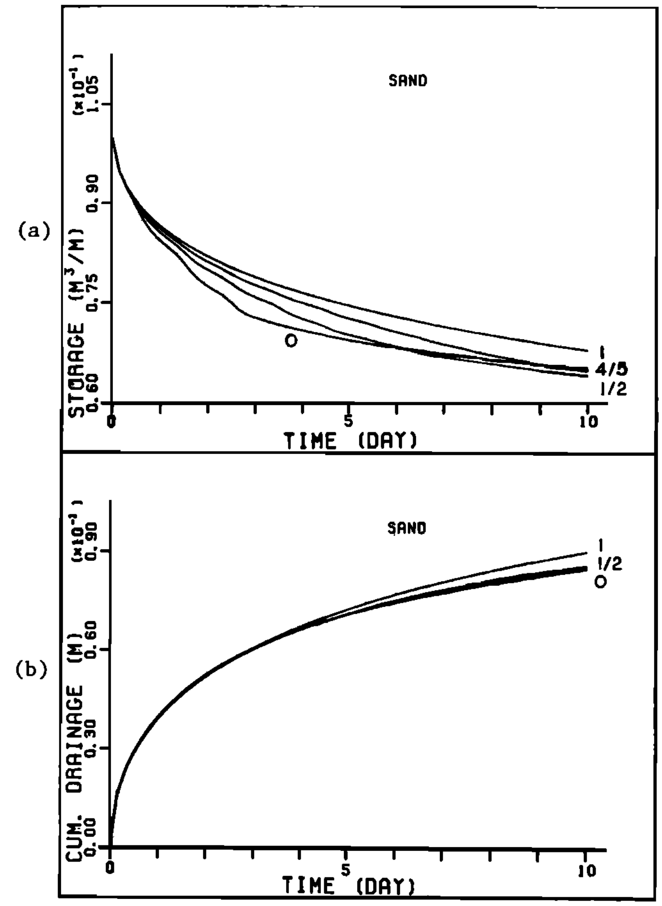

Fig. 9. Predicted water storage in the 0.35 × 1.0 m flow region in unit thickness (*a*) and cumulative drainage across the bottom boundary (*b*) for the sand soil with variable mulch width.

changes rapidly near the bare soil-mulch interface on the soil surface as shown in Figure 5*a*. At day 5, temperature contour lines near the right, upper corner are very dense, indicating rapid temperature change near the corner. Bare soil had high temperatures. Beyond day 5 the temperature distribution at 2:00 P.M. on each remaining day does not change much from Figure 7*b*. Table 3 shows the daily totals of the components of the surface energy balance and the maximum and minimum temperature on the bare soil surface (node 8) of the sand soil with a half-width mulch cover.

Simulations were made for repetitive evaporation and infiltration on the soil surface. Rainfall started at the beginning of day 3 and lasted for 6 hours with a total rainfall amount of 0.08 m. During the rainfall event, soil surface temperature was set equal to the air temperature. Though the outputs are not shown, the results of simulations with rainfall show that the rainfall reduces the previously very high soil surface temperature by supplying water for evaporation on the soil surface and that the rainfall delays the time period required for the surface to be very dry and to have high temperature.

Table 4 summarizes the daily total energy balances on day 1 and day 10 for each soil with or without mulch cover for the 10-day simulations of simultaneous evaporation and drainage. The components of the energy balance equation for mulched soil have nearly the same values regardless of soil type during the 10-day simulations. There are some differences in the values of the components for the bare soil surfaces. Energy partitioning was similar on days 1 and 10 for the clay bare surface. The sand and loam soil surfaces were dried by day 10, and the energy previously used for latent heat was shifted to sensible and soil heat.

Hydraulic Environment

The results of the soil heat and water movement simulation runs relating to the hydraulic environment are reported in this section. The results include soil water storage, drainage, evaporation, soil water content, and pressure head. The results of the 10-day simulations for the sand soil with a half-width mulch cover are reported.

Figure 8 shows the water content at the soil surface and the 5-cm depth for the sand soil with variable mulch width. The residual water content is reached and maintained at node 8 on the surface after days 3, 4, and 8 for a zero-, a half-, and a 4/5 width mulch, respectively. At the 5-cm depth node 8, water content first decreases to 0.15, then increases, as shown in Figure 8*d*. This is caused by reduced upward water loss due to the very small hydraulic conductivity near the soil surface while the soil receives moisture from below, resulting in positive net water flux at this position.

Figure 9 shows the soil water storage and the cumulative drainage for the sand soil with variable mulch width. Figure 9*a* shows that the fraction of mulch cover affects the soil water storage. Soil water storage is affected by mulches mainly through the effect of mulch cover on soil water evaporation. Figure 9*b* shows that the rate of drainage across the bottom boundary decreases exponentially in all of the mulch conditions.

Contour plots of soil water content and pressure head for the sand soil with a half-width mulch are shown in Figure 7. Near the bare soil surface the water contents are close to the residual water content, and the suction heads are very large from day 5.

Table 5 shows the daily totals of evaporation, drainage, and the maximum and minimum water content and pressure head on the bare soil surface (node 8) of the sand soil with a half-width mulch cover. Rainfall is an important contributor to soil water movement. In this study, all the 0.08 m of rainfall for the 6 hours on day 3 is infiltrated into the soil. Though the outputs are not shown, the rainfall changes water content and pressure head near soil surface abruptly. It raises the evaporation rate and the volume of water stored in the flow region. It also increases the drainage rate when the infiltrated water reaches the bottom boundary.

Table 6 summarizes the daily total water balance for differ-

TABLE 5. Daily Totals of Evaporation (*E*), Drainage (*D*), and the Maximum and Minimum Water Content and Pressure Head on the Bare Soil Surface (Node 8) of the Sand Soil With a Half-Width Mulch Cover

Day	E, mm	D, mm	θ_{max}, m³/m³	θ_{min}, m³/m³	h_{max}, m	h_{min}, m
1	4.74	37.72	0.206	0.155	−1.15	−2.04
2	4.75	12.85	0.185	0.124	−1.44	−3.11
3	4.70	8.40	0.160	0.085	−1.91	−6.41
4	4.78	6.20	0.118	0.005	−3.45	−1280
5	0.101	4.85	0.004	0.001	−1920	−18000
6	0.019	3.94	0.002	0.001	−6340	−19100
7	0.018	3.29	0.002	0.001	−7200	−18400
8	0.017	2.81	0.002	0.001	−6910	−18300
9	0.015	2.45	0.002	0.001	−7960	−18990
10	0.012	2.17	0.002	0.001	−8690	−18850

TABLE 6. Daily Total Water Balance in the 0.35 × 1.0 m Flow Region With Unit Thickness on Day 1 and 10 for Various Surface Mulch Widths With Simultaneous Evaporation and Drainage for a 10-Day Simulation

		Day 1			Day 10		
Soil	Mulch	Evaporation, 10^{-3} m^3	Drain, 10^{-3} m^3	Storage,* 10^{-3} m^3	Evaporation, 10^{-3} m^3	Drain, 10^{-3} m^3	Storage,* 10^{-3} m^3
Clay	0	1.67	7.87	165.20	1.79	0.61	132.87
	1/2	0.86	7.92	166.02	1.01	0.83	140.52
	4/5	0.38	7.95	166.47	0.46	1.00	144.23
	1	0.05	7.98	166.80	0.07	1.14	146.76
Loam	0	1.75	11.92	122.60	0.05	0.78	90.29
	1/2	0.96	11.93	123.61	1.13	0.95	92.28
	4/5	0.41	11.93	124.16	0.55	1.11	97.48
	1	0.05	11.94	124.55	0.07	1.25	100.78
Sand	0	1.68	13.20	85.22	0.001	0.78	65.30
	1/2	1.21	13.20	85.69	0.030	0.76	64.13
	4/5	0.60	13.20	86.30	0.077	0.84	65.81
	1	0.05	13.20	86.85	0.063	0.95	67.96

*At the end of each day.

ent soil surfaces in the 0.35 × 1.0 m flow region in unit thickness on day 1 and day 10 for the 10-day simulations. As the fraction of the mulch width becomes larger, the daily evaporation becomes smaller as long as enough moisture is supplied to the soil surface. On the other hand, as the fraction of the mulch width becomes larger, the daily drainage becomes greater also. However, the effect of mulch cover on evaporation seems more important than drainage for causing differences in water storage. The effect of mulch cover on water storage at the end of the 10-day simulations was greater for the clay and loam soils than for the sand soil.

CONCLUSIONS

An ADI method was developed and used to make predictions of soil surface energy paritioning and of soil heat and water movement in a two-dimensional flow region with partial soil surface mulch cover. The conclusions based on the present simulation study are as follows:

1. The net radiation heat flux is much smaller and the sensible heat flux is much greater on the mulch than on the bare soil surface when the soil surface is relatively wet.

2. The net radiation energy is partitioned mainly to latent heat as long as the soil surface is relatively wet. It is used mainly for sensible and soil heat when the soil surface is dry.

3. The soil surface temperatures are very high when the soil surface approaches its residual water content because incoming net radiation is used to heat up the soil surface instead of to evaporate soil surface moisture.

4. The amplitudes of daily temperature, water content, and pressure head variation under the mulch are much smaller than those on the bare soil surface.

5. The amplitudes of daily temperature, water content, and pressure head variation decrease rapidly as soil depths increase.

6. The soil heat and water flow is nearly one-dimensional below a soil depth of 40 cm.

7. The lateral heat and water flows near the soil surface with a partial mulch cover are significant.

8. The mulch cover suppresses the soil water evaporation to a large extent.

9. The mulch cover has only small impact on soil water drainage. Therefore, the mulch effect on the storage in the flow region is mostly governed by evaporation.

10. The partial mulch cover does not have a large effect on the water content at the 5-cm depth (node 8), where the plant seeds are located, during the 10-day simulation periods.

11. The mulch cover width effects on the 5-cm-depth, bare (node 8) soil temperature are small in the clay and loam soil and are large in the sand soil during a 10-day simulation.

12. The changes in the soil thermal and hydraulic environments are most rapid in the sand soil, followed by the loam soil and the clay soil.

The present ADI model has a wide application in soil science and groundwater hydrology and can be extended in many different ways. The exclusion of a vapor phase transport from the heat and water flow model may cause some discrepanices from the actual soil systems, especially for very dry soil conditions. This must be studied in the future.

NOTATION

A amplitude of daily temperature variation (°C).
a parameter in water retention equation (m^{-1}).
al soil surface albedo.
C volumetric soil heat capacity (J/m^3 °C).
c_{pa} specific heat of air at constant pressure (J/kg °C).
c_{ps} specific heat of soil at constant pressure (J/kg °C).
$D_{\theta v}$ isothermal vapor diffusivity (m^2/s).
DL day length (s).
DR daily global radiation (J/m^2).
E evaporation rate (m/s).
F $d\theta/dh$, specific water capacity (m^{-1}).
f porosity of mulch (m^3/m^3).
G soil heat flux (W/m^2).
g gravitational acceleration (m/s^2).
H relative humidity.
H_a air humidity (kg/m^3).
H_0 air humidity at soil surface (kg/m^3).
H_0* saturation humidity at the soil surface temperature (kg/m^3).
H_s sensible air heat flux (W/m^2).
h pressure (suction) head (m).
K hydraulic conductivity (m/s).
K_s saturated hydraulic conductivity (m/s).
L volumetric latent heat of vaporization (J/m^3).
LE latent heat flux (W/m^2).
M_s mulch heat flux (W/m^2).
n parameter in water retention equation.

R_g global radiation (W/m^2).
R_n net radiation (W/m^2).
R_1 long-wave sky irradiance (W/m^2).
r_a aerodynamic boundary layer resistance (s/m).
r_m the diffusion resistance of mulch layer (s/m).
SN solar noon (S).
T temperature (°C).
t time (s).
T_a air temperature (°C).
T_d dewpoint temperature (°C).
T_m mulch surface temperature (°C).
T_s soil surface temperature (°C).
THK thickness of mulch (m).
W_s wind speed (m/s).
x horizontal coordinate, positive to the right (m).
x_s volume fraction of solids in the soil.
x_0 volume fraction of organic matter in the soil.
z vertical coordinate, positive downward (m).
Z_0 soil surface roughness length (m).
α thermal diffusivity (m^2/s).
Δx x direction space step size (m).
Δz z direction space step (m).
Δt time step size (s).
ε emissivity.
θ volumetric water content (m^3/m^3).
θ_1 volumetric liquid water content (m^3/m^3).
θ_r residual water content (m^3/m^3).
θ_s saturation water content (m^3/m^3).
λ thermal conductivity of soil (W/m °C).
λ_m thermal conductivity of mulch layer (W/m °C).
ρ_a density of air (kg/m^3).
ρ_s density of soil (kg/m^3).
σ Stefan-Boltzmann constant (W/m^2 °K^4).
μ viscosity of liquid water (poise).
ω angular frequency (rad/s).
∇ gradient operator.

Acknowledgments. Journal paper J-12213 of the Iowa Agriculture and Home Economics Experiment Station, Ames, Iowa, Projects 2556 and 2715.

REFERENCES

De Vries, D. A., Simultaneous transfer of heat and moisture in porous media, *Eos Trans. AGU*, *39*, 909–916, 1958.

De Vries, D. A. Thermal properties of soils, in *Physics of Plant Environment*, edited by W. R. Van Wijk, North Holland, Amsterdam, 1963.

Forsythe, W. E., Smithsonian physical tables, *Smithson. Inst. Publ.*, *4169*, 827, 1964.

Gilding, B. H., The soil-moisture zone in a physically-based hydrologic model, *Adv. Water Resour.*, *6*, 36–43, 1983.

Haverkamp, R., and M. Vauclin, A note on estimating finite difference interblock hydraulic conductivity values for transient unsaturated flow problems, *Water Resour. Res.*, *15*, 181–187, 1979.

Haverkamp, R., M. Vauclin, J. Touma, P. J. Wierenga, and G. Vachaud, A comparison of numerical simulation models for one-dimensional infiltration, *Soil Sci. Soc. Am. J.*, *41*, 285–294, 1977.

Hillel, D., and C. H. M. van Bavel, Simulation of profile water storage as related to soil hydrologic properties, *Soil Sci. Soc. Am. J.*, *40*, 807–815, 1976.

Hillel, D. I., C. H. M. van Bavel, and H. Talpaz, Dynamic simulation of water storage in fallow soil as affected by mulch of hydrophobic aggregates, *Soil Sci. Soc. Am. Proc.*, *39*, 826–833, 1975.

Horton, R., and P. J. Wierenga, The effect of column wetting on soil thermal conductivity, *Soil Sci.*, *138*, 102–108, 1984.

Horton, R., O. Aguirre-Luna, and P. J. Wierenga, Observed and predicted two-dimensional soil temperature distribution under a row crop, *Soil Sci. Soc. Am. J.*, *48*, 1147–1152, 1984*a*.

Horton, R., O. Aguirre-Luna, and P. J. Wierenga, Soil temperature in a row crop with incomplete surface cover, *Soil Sci. Soc. Am. J.*, *48*, 1225–1232, 1984*b*.

Incropera, F. P., and D. P. DeWitt, *Fundamentals of Heat Transfer*, John Wiley, New York, 1981.

Jury, W. A., and B. Bellantuoni, Heat and water movement under surface rocks in a field soil: I. Thermal effects, *Soil Sci. Soc. Am. J.*, *40*, 505–509, 1976*a*.

Jury, W. A., and B. Bellantuoni, Heat and water movement under surface rocks in a field soil: II. Moisture effects, *Soil Sci. Soc. Am. J.*, *40*, 509–513, 1976*b*.

Lapidus, L., and G. F. Pinder, Numerical solution of partial differential equations in science and engineering, Wiley-Interscience, New York 1982.

Mahrer, Y., Prediction of soil temperature of a soil mulched with transparent polyethylene, *J. Appl. Meteorol.*, *18*, 1263–1267, 1979.

Mahrer, Y., and J. Katan, Spatial soil temperature regime under transparent polyethylene mulch: Numerical and experimental studies, *Soil Sci.*, *131*, 82–87, 1981.

Mahrer, Y., O. Naot, E. Rawitz, and J. Katan, Temperature and moisture regimes in soils mulched with transparent polyethylene, *Soil Sci. Soc. Am. J.*, *48*, 362–367, 1984.

Milly, P. C. D., Moisture and heat transport in hysteretic, inhomogeneous porous media: A matric head-based formulation and a numerical model, *Water Resour. Res.*, *18*, 489–498, 1982.

Milly, P. C. D., A simulation analysis of thermal effects on evaporation from soil, *Water Resour. Res.*, *20*, 1087–1098, 1984.

Philip, J. R., The theory of infiltration: 1. The infiltration equation and its solution, *Soil Sci.*, *83*, 345–357, 1957.

Philip, J. R., and D. A. De Vries, Moisture movement in porous materials under temperature gradients, *Eos Trans. AGU*, *38*, 222–232, 1957.

Schnabel, R. R., and E. B. Richie, Calculation of internodal conductances for unsaturated flow simulations: A comparison, *Soil Sci. Soc. Am. J.*, *48*, 1006–1010, 1984.

Selim, H. M., and D. Kirkham, Unsteady two-dimensional flow of water in unsaturated soils above an impervious barrier, *Soil Sci. Soc. Am. Proc.*, *37*, 489–495, 1973.

Sophocleous, M., Analysis of water and heat flow in unsaturated-saturated porous media, *Water Resour. Res.*, *15*, 1195–1206, 1979.

Van Bavel, C. H. M., and D. I. Hillel, A simulation study of soil heat and moisture dynamics as affected by a dry mulch, in *Proceedings 1975 Summer Computer Simulation Conference, San Francisco, CA*, pp. 815–821, Simulation Councils, Inc., La Jolla, California, 1975.

Van Bavel, C. H. M., and D. I. Hillel, Calculating potential and actual evaporation from a bare soil surface by simulation of concurrent flow of water and heat, *Agric. Meteorol.*, *17*, 453–476, 1976.

Van Genuchten, M. T., A closed-form equation for predicting the hydraulic conductivity of unsaturated soils, *Soil Sci. Soc. Am. J.*, *44*, 892–898, 1980.

Van Wijk, W. R., and D. A. De Vries, Periodic temperature variations in a homogeneous soil, in *Physics of Plant Environment*, edited by W. R. Van Wijk, North Holland, Amsterdam, 1963.

Wierenga, P. J., D. R. Nielsen, and R. M. Hagan, Thermal properties of a soil based upon field and laboratory measurements, *Soil Sci. Soc. Am. Proc.*, *33*, 354–360, 1969.

S.-K. Chung, Department of Agricultural Engineering, Kyungpook National University, Kyungpook, Korea.

R. Horton, Department of Agronomy, Iowa State University, Ames, IA 50011.

(Received February 9, 1987;
revised September 2, 1987;
accepted September 8, 1987.)